Geoelectric Characterization of Thermal Water Aquifers Using 2.5D Inversion of VES Measurements

Á. Gyulai, P. Szűcs, E. Turai, M. K. Baracza & Z. Fejes

Surveys in Geophysics
An International Review Journal
Covering the Entire Field of Geosciences and Related Areas

ISSN 0169-3298

Surv Geophys
DOI 10.1007/s10712-016-9393-z

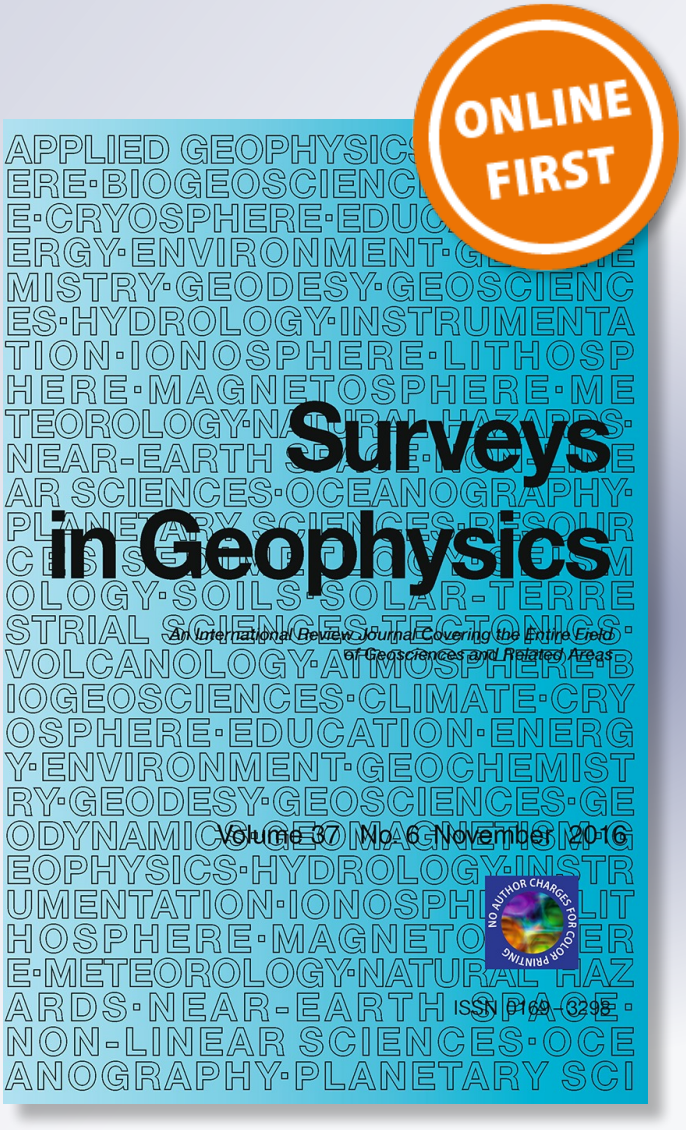

Springer

Surv Geophys
DOI 10.1007/s10712-016-9393-z

Geoelectric Characterization of Thermal Water Aquifers Using 2.5D Inversion of VES Measurements

Á. Gyulai[1] · P. Szűcs[1,2] · E. Turai[1] · M. K. Baracza[1] · Z. Fejes[1]

Received: 18 January 2016 / Accepted: 21 October 2016

Abstract This paper presents a short theoretical summary of the series expansion-based 2.5D combined geoelectric weighted inversion (CGWI) method and highlights the advantageous way with which the number of unknowns can be decreased due to the simultaneous characteristic of this inversion. 2.5D CGWI is an approximate inversion method for the determination of 3D structures, which uses the joint 2D forward modeling of dip and strike direction data. In the inversion procedure, the Steiner's most frequent value method is applied to the automatic separation of dip and strike direction data and outliers. The workflow of inversion and its practical application are presented in the study. For conventional vertical electrical sounding (VES) measurements, this method can determine the parameters of complex structures more accurately than the single inversion method. Field data show that the 2.5D CGWI which was developed can determine the optimal location for drilling an exploratory thermal water prospecting well. The novelty of this research is that the measured VES data in dip and strike direction are jointly inverted by the 2.5D CGWI method.

✉ M. K. Baracza
baracza@uni-miskolc.hu

Á. Gyulai
gfgyulai@uni-miskolc.hu

P. Szűcs
hgszucs@uni-miskolc.hu

E. Turai
gfturai@uni-miskolc.hu

Z. Fejes
fzolee14@gmail.com

[1] Faculty of Earth Science and Engineering, University of Miskolc, Miskolc-Egyetemváros 3515, Hungary

[2] MTA-ME Research Group of Geoengineering, University of Miskolc, Miskolc-Egyetemváros 3515, Hungary

Published online: 16 November 2016

Keywords Hydrogeology · Geological structures · Joint inversion · Series expansion-based inversion · Parameter estimation

1 Introduction

Geoelectric methods have widespread use in engineering, geophysical, geological and hydrogeological, geotechnical and environmental studies. Some of them have been developed suitably for the investigation of complex heterogeneous structures. For prospecting 2D/3D structures, finite difference (FD), finite element (FE), integral equation and analytical and approximate methods have been developed. The method of 1D approximation is often used for solving the forward and inverse problems (summarized in Koefoed and Mallick 1979). Geoelectric methods are widely used in hydrogeological investigations all over the world (Buvat et al. 2013; Gandomi and Binley 2013; Olainka and Weller 1997; Bortoloza et al. 2011). It is also evident, however, that to refine the research additional methods must be developed, such as joint inversion, qualification of the inversion method and application of 2D and 3D evaluations. In practice, the 1D approximation can only be applied in the determination of 2D/3D structures when the thicknesses and resistivities of layers vary relatively smoothly and slowly. In the opposite case, fast variations of the model parameters may cause problems (Beard and Morgan 1991; Meheni et al. 1996). A single inversion method is commonly used in 1D approximation. In that case, not only the error of approximation but also the inaccuracies of the single inversion procedure (e.g., ambiguity) bear great influence on the evaluation results. Joint inversion methods have been developed to improve the inversion results (Vozoff and Jupp 1975; Dobróka et al. 1991; Hering et al. 1995; Gyulai and Ormos 1996; Misiek et al. 1997; Haber and Oldenburg 1997; Kis et al. 1998; Gallardo and Meju 2004; Szabó 2004; Dobróka and Szabó 2005; Jegen et al. 2009; Dobróka et al. 2009; Doetsch et al. 2010; Gyulai et al. 2012, 2013; Gyulai and Szabó 2014; Szabó 2015).

Several approaches have been taken toward improving the accuracy of the interpretation results required of geoelectric exploration. This paper emphasizes certain development tendencies and does not consider those researches that are based on the transformation of geoelectric data measured in one layout to that of another one (e.g., from Wenner array to Schlumberger array) (Kumar and Das 1978). One of the most important results in the development of 2D/3D geoelectric forward modeling methods was published by Mufti (1976) and Dey and Morison (1979a, b). They allowed the researchers to use procedures more accurate than 1D approximation for inverse modeling. The original and further developed releases of Spitzer's (1995) algorithm (and software) represent an outstanding procedure, which is integrated in the suggested series expansion-based inversion method. The implementation of FD methods has been an important step to a more accurate interpretation (Tripp et al. 1984; Barker 1992; Li and Oldenburg 1994; Loke and Barker 1996), while the application of integral equation methods (Lee 1975) and the development of FE methods (Coggon 1971; Sasaki 1994; Günter et al. 2006) have also been of great importance in finding a better interpretation. Analytical procedures have been worked up for solving 2D forward modeling problems (Alpin et al. 1966; Gyulai and Ormos 1996).

2 Interpretation of VES Data Using Series Expansion-Based Inversion Method

Direct current (DC) surveys are frequently used in geoelectric exploration. One of them, the multi-electrode measurement technique, using several types of arrays, can be easily adapted for shallow investigation purposes down to a depth of 20–30 m. The application of the method is advantageous because of a quick computerized data acquisition process, high density of apparent resistivity data collected in both horizontal and vertical directions and relatively simple interpretation of resistivity pseudosections. Moreover, the reconstruction of complicated (rapidly varying) geological structures can be made by inversion-based tomographic imaging methods (Loke and Barker 1996; Geotomo Software: Res2DINV 2006; Gyulai and Ormos 1999; Auken and Christiansen 2004; Auken et al. 2005; Blaschek et al. 2008). Despite the abundance of data collected from a multiply overlapped area, it is necessary to apply smoothness constraints on the multitude of unknown model parameters so as to regularize the inversion procedure. Hence, it arises that the inversion procedure becomes stable, but there is no possibility to check the reliability of inversion estimates based on the model covariance matrix (Menke 1984). It is also obvious that the determination of resistivity for a given volume of rock may be helpful in setting an initial model. The most challenging problem of the Res2DINV algorithm is the rather limited in estimation accuracy when it is used for the inversion of VES (vertical electrical sounding) data observed along the line of VES stations with a separation of 50–500 m and different penetration depths between 100 and 500 m. In the lateral direction, the structures are not covered quite densely by the volumetric elements because of the sparse data set.

2.1 Geoelectric Inversion Method Using Series Expansion

In geoelectric series expansion-based inversion, the variations of geometrical (i.e., layer boundary) and physical (i.e., resistivity) parameters of the geological structure are described by continuous functions expanded into series along the profile. Then, the series expansion coefficients are estimated in the inversion procedure to derive the physical and geometrical parameters. (In 3D inversion, bivariate basis functions are used in the series expansion.) In the inversion practice, Fourier expansion has been mostly applied for the discretization of laterally changing model parameters (Gyulai and Ormos 1999)

$$\rho_n(s) = \frac{1}{2} d_{n_o} + \sum_{k=1}^{Kn} d_{n_k} \cos k \frac{2\pi s}{s_p} + \sum_{k=1}^{Kn} d^*_{n_k} \sin k \frac{2\pi s}{s_p}, \tag{1}$$

$$h_n(s) = \frac{1}{2} c_{n_o} + \sum_{l=1}^{Ln} c_{nl} \cos l \frac{2\pi s}{s_p} + \sum_{l=1}^{Ln} c^*_{n_l} \sin l \frac{2\pi s}{s_p}, \tag{2}$$

where index $n = 1, 2, \ldots, N$ runs through the number of layers (N is the total number of layers), $\rho_n(s)$ is the resistivity function of the nth layer, $h_n(s)$ is the thickness function of the nth layer, s is the lateral coordinate along the profile, S_p is the total length of the profile and $d_{n_k}, d^*_{nk}, c_{n_l}, c^*_{n_l}$ denote the expansion coefficients, respectively. Constant K_n and L_n can be determined on the basis of the VES measuring stations. The maximum values of parameters K_n and L_n are determined by the number of VES stations as is stated by Gyulai and Ormos (1999).

2.1.1 1.5D Geoelectric Inversion Method

In the first phase of the interpretation procedure, the 1.5D inversion method is used. Data prediction is based on a 1D forward modeling algorithm, which gives a quick estimate of the initial model and then of the apparent resistivities calculated with the modified model. The 1.5D inversion procedure requires barely more CPU time than the whole set of 1D inversion procedures. The least squares (LSQ) method is used in the linearized inversion algorithm. Gyulai and Ormos (1999) derived the covariance matrix for the case of laterally varying geoelectric models, which characterizes the reliability of the inversion procedure. Owing to the 1D approximation, it necessarily follows that reliability can be quantified only approximately via the estimation errors calculated in the 1.5D inversion procedure.

2.1.2 Combined Geoelectric Inversion (CGI) Method

The CGI method is discussed in detail by Gyulai et al. (2010). The inversion algorithm is comprised of two phases. In the first step, the initial model used for the succeeding time-consuming 2D inversion procedure is estimated by a rapid 1.5D inversion method, which provides a proper solution after a few iteration steps. In the relevant paper, the data distance d, model distance D, estimation error σ_{k_m} (uncertainty), average estimation error F and correlation norm S have been defined, respectively.

Various quantities can be used to characterize the accuracy of the inversion results. In the data space, the normalized data distance d is defined

$$d = \sqrt{\frac{1}{I}\sum_{i=1}^{I}\left(\frac{\rho_{a,i}^{(\text{observed})} - \rho_{a,i}^{(\text{calculated})}}{\rho_{a,i}^{(\text{calculated})}}\right)^2} \times 100\%, \tag{3}$$

where I denotes the total number of apparent resistivity data ρ_{ai}. In the case of inversion of synthetic data calculated on an exactly known model (with model parameters $\vec{m}^{(\text{exact})}$), the relative model distance has been computed

$$D = \sqrt{\frac{1}{M}\sum_{i=1}^{M}\left(\frac{m_i^{(\text{estimated})} - m_i^{(\text{exact})}}{m_i^{(\text{exact})}}\right)^2} \times 100\%, \tag{4}$$

where M is the total number of model parameters.

The accuracy of the parameter estimation is often characterized by means of the variances, which are derived from the diagonal elements of the parameter covariance matrix (Menke 1984). We give the elements of the covariance matrix at each VES station by using the formulation of series expansion, which is a new solution for lateral changes. Since the covariance matrix is calculated primarily to the expansion coefficients in the inversion procedure, the covariance matrix of the layer parameters is estimated in a new step in the practice

$$\sigma_{km} = \sigma_k(x_m) = \frac{\sqrt{\sum_{i=1}^{J(k)}\sum_{j=1}^{J(k)}\left\{\Psi_{ki}(x_m) \times \Psi_{kj}(x_m) \times COV_{ij}\right\}}}{p_k(x_m)}, \tag{5}$$

where $\sigma_k(x)$ denotes the estimation error of the kth model parameter (i.e., resistivity or thickness) and σ_{km} is the same at the mth VES station (at $x = x_m$). K is the total number of the $p_k(x)$ model parameters ($k = 1, 2, \ldots, K$), and M is the number of VES stations along

the profile ($m = 1, 2, \ldots, M$). $J(k)$ is the number of basis functions in the series expansion describing the kth model parameter, $\Psi_{ki}(x)$ and $\Psi_{kj}(x)$ are the ith and jth basis functions and COV_{ij} is the covariance matrix elements of the estimated expansion coefficients (Menke 1984).

In order to give an overall accuracy of the parameter estimation for the whole model, the mean (percentage) estimation error F is introduced as

$$F = \sqrt{\frac{1}{KM}\sum_{k=1}^{K}\sum_{m=1}^{M_k}\sigma_{km}^2} \times 100\,(\%). \tag{6}$$

In order to characterize the degree of correlation among the estimated model parameters, the Pearson's correlation matrix is extensively used

$$\mathrm{CORR}_{ij} = \frac{\mathrm{COV}_{ij}}{\sqrt{\mathrm{COV}_{ii}\mathrm{COV}_{jj}}}. \tag{7}$$

Because of the large number of the matrix elements, it is useful to introduce a single scalar

$$S = \sqrt{\frac{1}{P(P-1)}\sum_{j=1}^{P}\sum_{i=1}^{P}\left(\mathrm{CORR}_{ij} - \delta_{ij}\right)^2}, \tag{8}$$

called the mean spread (Menke 1984), as a general characteristic value describing the model correlation (P is the total number of the model parameters; δ_{ij} is the Kronecker delta). The smaller the values of D, F and S characterizing the whole inverted section (which is calculated from the covariance matrix of expansion coefficients), the more reliable are the results of the 1.5D and CGI. In the inversion of field data, only F and S can be used for the characterization of the inversion results. For investigations using synthetic data, we can additionally use the model distance D. These values can be applied for the determination of the optimal number of coefficients (Gyulai et al. 2010).

A strategy for the determination of the optimal number of expansion coefficients is also suggested, presented as one of the most important problems of the series expansion-based inversion method. According to this strategy, the highest possible numbers of expansion coefficients (i.e., most complicated geological model) are accepted as a solution of the inverse problem, where the misfit between the observed and predicted (for the model) data (d) and the average estimation error (uncertainty) F are simultaneously minimal. All these inversion results were presented as synthetic and case studies. The CGI results were compared to those of the Res2DINV software by using synthetic modeling examples. A case study including the evaluation of a laterally slowly varying model was shown to make a comparison between the 1.5D inversion and CGI methods. The two methods gave similar results, with the difference that the estimation errors were significantly reduced by the CGI method.

2.1.3 *Combined Geoelectric Weighted Inversion Over a Two-Dimensional Geologic Structure*

Drahos (2008) published a joint inversion method for processing data following Gaussian distribution, which is based on the automatic weighting of geophysical data sets. The 2.5D combined geoelectric weighted inversion (CGWI) method fulfills the above requirement by using automatic weighting on the measurement data. As a result, the reliability of

parameter estimation is not reduced (or improved just slightly) when data sets burdened with large errors are inverted. This can be made easily by using the CGWI method, which allows for each VES station situated along a profile to have different amounts of uncertainty. No preliminary knowledge of the errors is required as the inversion algorithm estimates them automatically.

Gyulai et al. (2014) successfully applied the aforementioned automated weighting procedure in the CGWI framework. A field study was shown to demonstrate the significant differences between the estimation errors (F) given by 1D single inversion and 2D CGI methods. The study draws attention to the estimation errors given by the 1D inversion procedure that sometimes exceed 100%.

2.1.4 2.5D Geoelectric Inversion Method Using Series Expansion

Gyulai and Tolnai (2012) presented the principles of a new approximate inversion method used for the determination of 3D geological structures. The principles of the series expansion-based geoelectric inversion method are detailed in Gyulai et al. (2010). In this study, the 2.5D CGWI procedure is further developed and applied to the interpretation of real data. The workflow of the inversion process is shown in Fig. 1.

In our previous papers, 3D approximate methods using measurements with two different directions were presented. It was assumed that the direction of dip and strike is known. In the knowledge of the main directions of the structure, one can apply either a dip or a strike direction forward modeling procedure. The Steiner's most frequent value method takes the deviation from the 2D structure into consideration with using an automatic weighting of data. The new method assumes that the geological structure may vary in both directions,

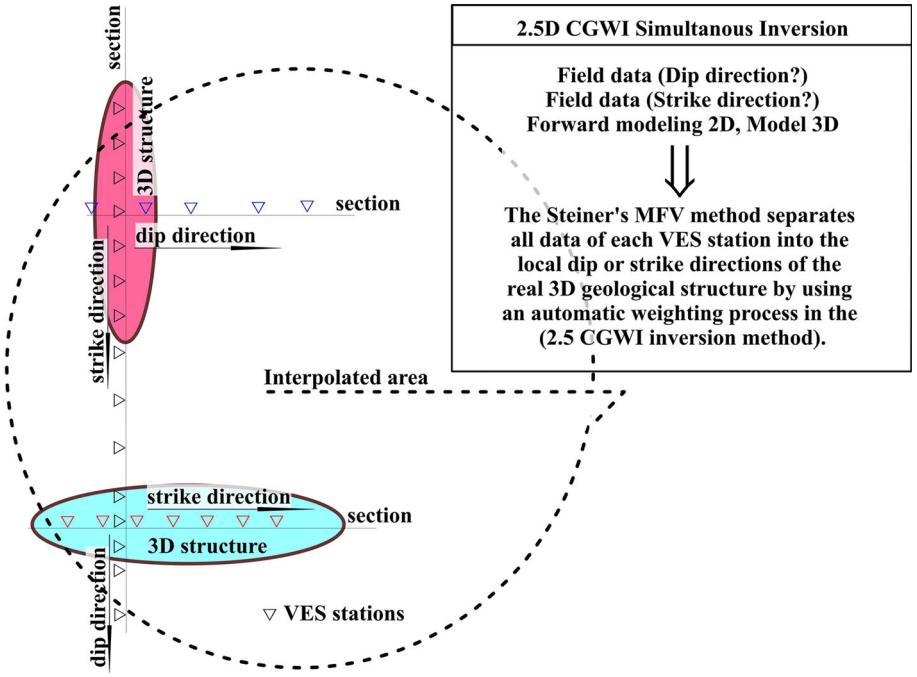

Fig. 1 Workflow of 2.5D CGWI

i.e., the data of VES stations along a profile or that of the same VES station can be more like dip or strike type. It is advisable to assume the appearance of both data types along the same profile. The Steiner's most frequent value (MFV) method allows for such separation of data measured along a section and the determination of the structure using a simultaneous inversion technique. Obviously, the proper resolution of 3D structures requires observations over a measurement grid. The newly suggested method reduces the 3D problem to a set of section-wise evaluations. Then, the vertical and horizontal variation of the geological structure is determined by the interpolation of the data of the sections. The concept of the series expansion-based 3D inversion method seems to be a promising step-forward for a more correct interpretation, but it may cause problems of increased computer time and less reliability of the results of complicated (multivariate) inversion procedure. As is shown in Fig. 1, there are two types of geological structures along Profile-I. One type follows dip direction and the other follows the strike direction; thus, some of the data of each VES station are either dip or strike direction measurements depending on the separation distance of the given VES array. However, before the measurement, we do not know which data belong to dip or strike direction and which the main directions of the geological structure are. Before the inversion phase, all input data are treated if they were dip and strike direction measurements. They are automatically separated only in the simultaneous 2.5D CGWI procedure. This separation is performed at every electrode distance of each VES station using the Steiner's MFV method using a special weighting process. This simultaneous inversion procedure is used to process the data of Profiles 0, I, II, III, respectively. The determination of the areal (spatial) distribution of layer parameters requires further interpolation.

The new inversion technique is more efficient than the one suggested earlier by Gyulai and Tolnai (2012), because it does not require the preliminary knowledge on the classification of the data (whether it is dip or strike direction type). The new inversion method forms the next step in the implementation of the 3D CGWI procedure. The measurement system meets the requirements of the 3D inversion procedure from the point of view that the 3D structure is measured along several directions. The joint inversion of data sets measured along the same profiles in different directions allows for making the 3D interpretation with adequate accuracy. The information contents of strike and dip direction measurements are aggregated in the 3D inversion procedure. Since the information matrices of data sets measured along several directions may differ from each other, this sort of linkage corresponds to a joint inversion process. However, the inversion result for the 3D model is as approximate as that of the 1.5D procedure for the 2D structure. The novelty of the new inversion method compared to 2.5D CGWI is the application of Steiner's weights (Steiner 1988, 1991, 1997), which allows for reducing the effect of outlying data in the 3D inversion procedure. The noise rejection capability of the robust MFV method was also shown for an inversion-based Fourier transformation method (Dobróka et al. 2016) and in statistical processing of well-logging data sets (Szabó and Balogh 2016). By using a combination of 2D and 3D synthetic models, Gyulai and Tolnai (2012) demonstrated that the 3D structure can be built up from 2D structural elements with higher accuracy. An exact series expansion-based 3D inversion method can be implemented by using bivariate (e.g., harmonic) basis functions. A part of this methodology, namely the bivariate series expansion, was previously used in gravity inversion by Dobróka and Völgyesi (2008).

The core of the inversion method is the application of Steiner's weights. According to Menke (1984), the normal equation of the weighted least squares method is

$$\mathbf{G^T W G p} = \mathbf{G^T W \rho}, \tag{9}$$

where **G** denotes the Jacobi's matrix, **W** is the weighting matrix, **p** is the (unknown) model vector and **ρ** is the vector of observed (input) data. The inversion algorithm using Steiner's weights has been applied successfully by Dobróka et al. (1991). The weighting matrix is calculated in an iterative procedure by using the most frequent value (MFV) method

$$W_{ij} = \begin{cases} \left(\dfrac{\varepsilon_{l+1}^2}{\varepsilon_{l+1}^2 + y_j^2} \right) & \text{if} \quad i = j \\ 0 & \text{otherwise} \end{cases}, \tag{10}$$

where y_j is the jth residual and the dihesion (Steiner's scale factor)

$$\varepsilon_{l+1}^2 = 3 \frac{\sum_{j=1}^{N} \frac{y_i^2}{\varepsilon_l^2 + y_j^2}}{\sum_{j=1}^{N} \frac{1}{\varepsilon_l^2} - y_j^2}, \tag{11}$$

is obtained from the value of ε_l^2 estimated in the previous iteration step (Steiner 1988). The initial value of ε_0 can be chosen as

$$\varepsilon_0 \leq \frac{\sqrt{3}}{2} (y_{\max} - y_{\min}). \tag{12}$$

By using the above weighting process, the outlying data are inverted with minimal amount of importance. As a result, they bear relatively small influence on the estimation result. The application of the Steiner's weighting process opens the door to solving the 3D inverse problem with an approximate 2.5D CGWI method. The question arises as to how one can avoid the mixing of dip and strike types of data along a profile (even in the same measurement direction) caused by the changing of the elongation directions of 3D structural elements. Unfortunately, which datum belongs more to dip direction than to strike direction is not known. The problem could be solved with the joint inversion of the dip and strike profiles. One must trust the separation of data to the special algorithm of Steiner. Gyulai and Tolnai (2012) showed that this solution may significantly improve the accuracy and reliability of the inversion processing of mixed data sets in the case of synthetic geoelectric models.

3 Application of 2.5D CGWI Method Using Field Data

3.1 Study Area and Geological Setting

The investigation site is located near the town of Szerencs, North-East Hungary (Kiss 2007). The measurement area was set out after a detailed analysis of airborne magnetic maps (data source: Geological and Geophysical Institute of Hungary) and data sets (data sources: National Institute for Environment and Geoservice Ltd) acquired from neighboring boreholes (Szűcs et al. 2013).

In the area, the aquifers are represented by rocks of volcanic origin (Székely et al. 2015). Hydroquarzite zones are formed by hot water flow through the fractures and fissures of the rhyolite, which are responsible for the up-flow of thermal water. At the northern part of the site, in the shallow region (from a spring in Bekecs), farther south at a depth of

approximately 200 m, warm (thermal) water is drawn from two or three wells. The uppermost 50- to 100-m-thick shaly complex with 10–15 Ω resistivity does not contain any permeable zone. The underlying rock is a weathered ashy sediment of shallow-water origin, the argillization of which prevents it from carrying thermal water. Toward the south, the fissured rhyolite deepens into the subsurface along fractured zones, where the thin hydroquarzite formations form aquiferous horizons. From the point of view of the geophysical exploration, it is assumed that a few 100 m away, southward, there are fractured volcanic (hydroquarzite) zones at a depth of at least 400 m, from which thermal water can be extracted at a temperature of 30 °C at the lowest estimate. The difficulty of this task is that the hydroquarzite zones of these depths cannot be detected directly by geoelectric methods. However, it is possible to investigate vent rocks, faults and fractures where thermal water up-flow can be expected.

The geophysical survey included traditional VES measurements the data of which were processed by quality-checked 2D CGI and/or 2.5D CGWI (approximate 3D) inversion methods. In first step of the 2.5D CGWI procedure, the 1.5D inversion approximation is applied. According to the inversion strategy, several attempts have been made for the estimation of the number of expansion coefficients using the quantities d and F (Gyulai et al. 2010). This phase includes 20 fast iterations. The resultant model obtained by the 1.5D inversion process is treated as an initial model of the 2.5D CGWI procedure. The latter comprised a further 10–15 iteration steps. Similarly, the 2D CGI of dip and strike data was earlier performed in two phases. This is not necessary for the 2.5D CGWI, but it is done for making a comparison between the inversion methods.

The location map of the thermal water prospecting site including the installed VES stations and producing wells is shown in Fig. 2a. The VES stations used for the areal survey were allocated with non-uniform spacing. Profile-0 defined by VES stations 1, 11, 14, 17 and 20 was designed for the characterization of the geological environment of the neighboring water wells including a dry well (with a bottom of 600 m) in the vicinity of station 20. Profile-I, referred to as a basic section, was constituted by VES stations 1–10, established for the exploration of fault and fracture zones. The anomalous zones in the west–east direction were detected by the measurements made along Profile-III including VES stations 6, 12, 15, 18 and 21 and Profile-II including VES stations 10, 13, 16, 19 and 22. To the north of VES station 18, there were two additional VES measurements made (2/6, 2/7) after the quick-look interpretation.

The vertical geological section including the producing wells drilled in the survey area is shown in Fig. 2b. This section provides information also on the traversed layers, the depth of the aquifers and other well test data. The depth of the deepest borehole (K-53) is approximately 600 m, from which it was not possible to produce thermal water.

3.2 Interpretation of Geoelectric Measurements

3.2.1 Measurement Data and Their 1D Inversion Evaluation of the VES Stations Denoted as Reference (REF)

The names of the VES stations denoted as reference (REF) stations were used in the very beginning of the investigation. For making a pilot survey, the VES profiles indicated by REF were planned next to the thermal wells operated for different purposes (REF1 located around wells B-3 and B-4, VES station 2 in the vicinity of well B-55 and REF3 not so far away from well CS-3). Since station REF2 is situated above a fault zone, the VES station 2 installed in the vicinity of well K-60 would have been preferably called REF2 in the

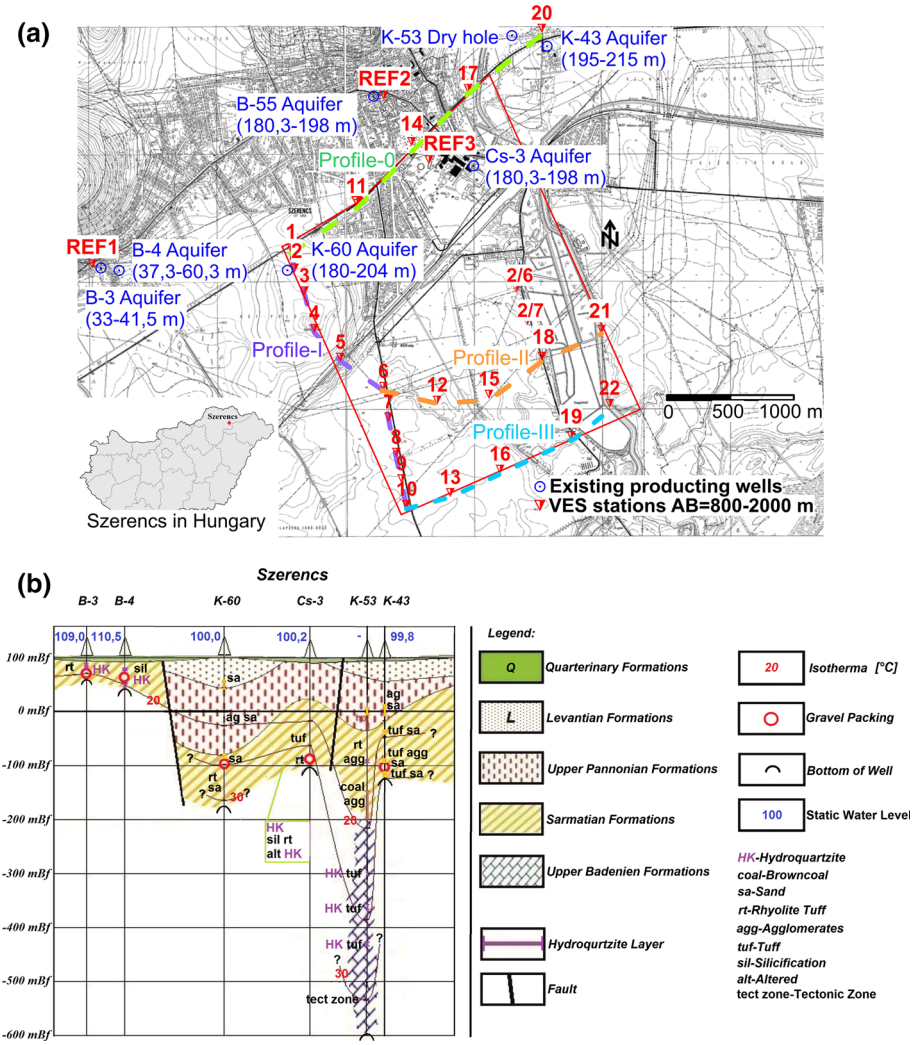

Fig. 2 **a** Location map of the thermal water prospecting site in Szerencs **b** Vertical section of the geological setting in Szerencs

knowledge of the VES curve of station REF2. Because of the architecture, VES station REF3 could only be located 150–200 m farther from well CS-3. The VES curves denoted by REF and their 1D interpretations are shown in Fig. 3 and Table 1, where the aquifer is indicated with relatively high resistivities. The aquifer zone including warm water can be detected by the qualitative interpretation of the VES curves and the layer sequences of the wells. The VES data observed at station REF1 show a good agreement with the depth of the hydroquartzite aquifer inferred from wells B-3 (33–41.5 m) and B-4 (37.3–60.3 m). REF2 is a typical VES station established on the top of a fault zone, which is clearly shown in Fig. 3. The presence of the aquifer at the depth of 180–190 m estimated by the 2.5D CGWI of data measured along Profile-I as part of the VES station 2 situated in the neighborhood of well K-60 is confirmed by the results of drilling information on a producible layer at 180–204 m (Fig. 6). The

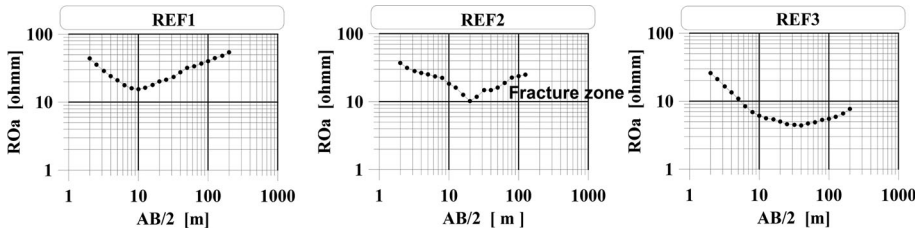

Fig. 3 REF1, REF2, REF3 VES curves

Table 1 Results of 1D inversion of REF1, REF2, REF3 VES stations

VES station	First layer thickness (m) h_1	Second layer thickness (m) h_2	Third layer thickness (m) h_3	First layer resistivity (Ω m) ρ_1	Second layer resistivity (Ω m) ρ_2	Third layer resistivity (Ω m) ρ_3	Fourth layer resistivity (Ω m) ρ_4
REF1	1.3	11.2	63.2	55.2	14.1	48.9	102
REF2	Fracture zone						
REF3	1.3	2.9	101.4	34.3	8.2	4.5	50

overburden is a low resistivity (around 5 Ω m) clayey zone without lateral movement of water. The aquifer is indicated with higher apparent resistivities in the VES curve. After completing the measurement and interpretation of VES stations named REF, the survey area was shifted southward by several 100 m. Because of the actual geothermic gradient, we assumed an investigation depth of 400 m.

3.2.2 Inversion Results of the Profile-I

Consider first the interpretation of Profile-I. Apparent resistivity data measured at VES stations 1–10 were plotted in double-logarithmic scale (Fig. 4).

Since the shapes of the sounding curves are fairly similar, the apparent resistivities of the layers are assumed to be hardly changed along the lateral direction. The single (1D) inversion of some apparent resistivity curves provides unreliable inversion results. The apparent resistivity pseudosection of Profile-I infers good structural variations in Fig. 5. Figure 5 shows a qualitative picture of the geological situation along Profile-I, which is worth comparing with the results of the 2.5D CGWI procedure (Fig. 6). This is the reason of showing the apparent resistivity pseudosection beside the inversion result.

In Fig. 5, the coordinates of AB/4 are identified as vertical depth. The shape of the 15-Ω m-thickened isoline shows the depth variation of the surface of the high-resistivity (rhyolite) basement (i.e., in the vicinity of VES station 2, the depth of the hydroquarzite-bearing rhyolitic tuff is around 200 m), which can reach a depth of 400 m in several segments of the profile. For instance, this is well marked at VES station 10. On the other hand, the depth of the hydroquarzitic rhyolite tuff is around 200 m in a nearby producing well in the vicinity of VES station 2. It can be seen even without inverse modeling that the dynamics of the lateral depth variation are significant, which meets our earlier expectations.

The occurrence of rift volcanism is inferred from the result of 2.5D CGWI procedure between VES stations 5–6 and 9–10, where the rift valley is filled with several 100-m-thick

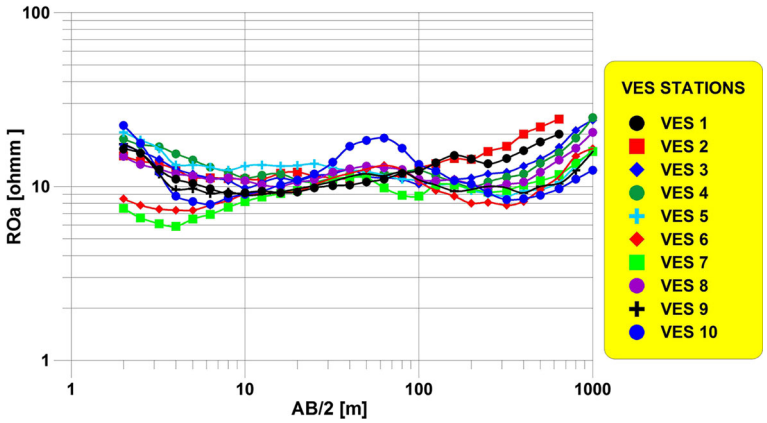

Fig. 4 Apparent resistivity curves measured at VES stations 1–10 along Profile-I by Schlumberger array

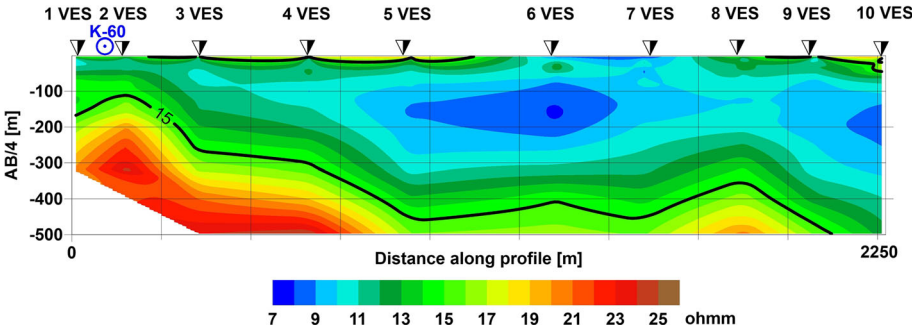

Fig. 5 Apparent resistivity pseudosection along Profile-I

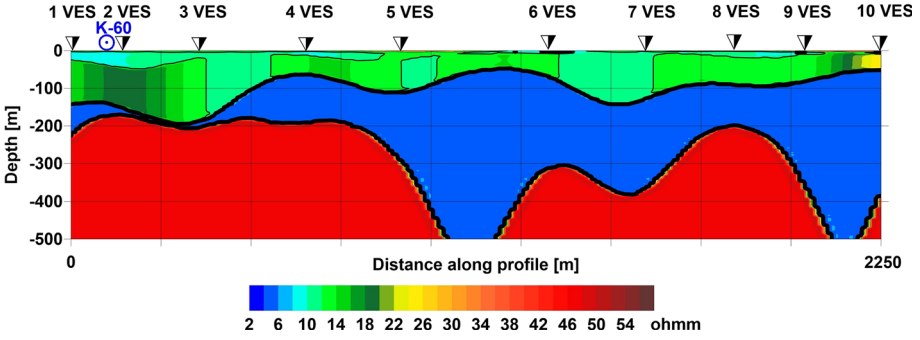

Fig. 6 Resistivity section estimated by 2.5D CGWI method along Profile-I

weathered tuff of 5–6 Ω m resistivity (Fig. 6; Table 2). The up-flow of thermal water is expected on both sides of the rifts.

The estimated parameters and their measurement units are resistivity ρ_i (Ω m) and layer thicknesses h_i (m). As Gyulai et al. (2010) defined, d is the normalized data distance, F is the mean estimation error, S is the correlation average and σ_{k_m} is the estimation error (within brackets). The relatively high F value is related to the high estimation errors of

Table 2 Results of 2.5D CGWI of VES data along Profile-I

	VES station 1	VES station 2	VES station 3	VES station 4	VES station 5	VES station 6	VES station 7	VES station 8	VES station 9	VES station 10
$d = 0.9\%$, $F = 47.6\%$, $S = 0.226$										
ρ_1	21.63 (12)	17.78 (35)	20.42 (29)	19.79 (18)	40.42 (12)	10.72 (4)	16.94 (38)	14.96 (14)	27.62 (12)	55.19 (2)
ρ_2	8.96 (78)	10.81 (64)	10.02 (49)	10.29 (42)	13.22 (100)	6.59 (139)	4.76 (17)	9.97 (18)	8.38 (105)	7.19 (160)
ρ_3	14.61 (48)	16.53 (6)	11.20 (59)	14.25 (16)	11.89 (157)	13.77 (76)	10.53 (82)	13.92 (30)	12.25 (59)	25.64 (49)
ρ_4	5.95 (48)	5.95 (14)	5.95 (33)	5.95 (26)	5.95 (57)	5.95 (60)	5.95 (74)	5.95 (47)	5.95 (142)	5.95 (175)
ρ_5	47.87 (3)	47.87 (2)	47.87 (5)	47.87 (10)	47.87 (29)	47.87 (30)	47.87 (17)	47.87 (10)	47.87 (14)	47.87 (11)
h_1	1.00 (11)	0.97 (25)	1.21 (12)	1.94 (9)	0.60 (52)	0.72 (27)	0.53 (25)	1.45 (16)	0.86 (21)	0.82 (9)
h_2	23.56 (4)	40.42 (2)	6.02 (6)	20.60 (2)	12.46 (7)	4.79 (5)	2.29 (13)	9.12 (3)	9.49 (2)	8.10 (2)
h_3	118.74 (1)	143.02 (2)	95.62 (0)	56.67 (1)	76.69 (3)	44.85 (1)	138.34 (1)	76.27 (1)	77.31 (0)	41.41 (1)
h_4	84.67 (2)	13.59 (26)	81.76 (3)	114.21 (1)	345.14 (1)	345.21 (1)	232.17 (1)	147.01 (1)	219.42 (1)	338.89 (0)

The numbers in parentheses indicate the error estimates

resistivities. One by one σ_{k_m} summarized in F and the correlation norm S are very important for evaluating the reliability of inversion estimates (note that values of σ_{k_m} and F are defined for the layer parameters, while S values are for the coefficients).

Table 3 compares the results of the different inversion methods investigated. It shows the numerical results of different inversion procedures, where 1D shows the result of 1D single inversion, 2D CGI dip gives the result of 2D CGI along dip direction, 2D CGI strike is the result of 2D CGI along strike direction and 2.5D CGWI is the result of 2.5D CGWI. Parameter Y^* is the mean estimation error of $H = h_1 + h_2 + h_3 + h_4$ referring to a given VES station (H denotes the depth of the hydroquarzitic rhyolite tuff)

$$Y^* = \sqrt{\frac{\sum_{n=1}^{N} \sigma_{nM}^2}{N}}, \tag{13}$$

where N is the number of layers, M is the number of model (VES station) and Y_n^* is the estimation error normalized to layer thicknesses referring to a given VES station

$$Y_n^* = \sqrt{\frac{\sum_{n=1}^{N} \sigma_{nM}^2 h_n}{\sum_{n=1}^{N} h_n}}, \tag{14}$$

where N is the number of layers and M is the number of the model.

It is worth mentioning that values of Y_n^* and Y^* greater than 100% do not quantify the estimation error, but only qualify the estimation's uncertainty. The deviation between the depths estimated separately by the 1D and 2.5D CGWI methods is not nearly as high as that shown by parameters Y_n^* and Y^*. This phenomenon is well known in quality-checked inversion, since derivation is the point feature of layer parameters.

The above analysis of the depth estimation is further analyzed in the "Appendix" (see Figs. 17, 18).

Table 3 Results of different investigated inversions for the Profile-I

VES stations	1D			2D CGI (dip)			2D CGI (strike)			2.5D CGWI		
	H (m)	Y_n^* (%)	Y^* (%)	H (m)	Y_n^* (%)	Y^* (%)	H (m)	Y_n^* (%)	Y^* (%)	H (m)	Y_n^* (%)	Y^* (%)
1	190**	980	940	211	13	56	287**	40	72	228	2	6
2	177*	1136	1061	189	26	105	196	22	180	198	4	18
3	211*	1409	1161	173	9	65	160*	11	27	185	2	7
4	196	260	208	219	3	20	185	10	19	193	1	5
5	320**	352	210	529**	12	130	547**	8	61	434	2	26
6	306**	28	86	336**	10	75	505*	9	276	395	1	13
7	460**	32	54	317*	6	61	309**	6	272	373	1	14
8	256	62	50	240	14	18	217	10	30	233	1	8
9	452**	55	35	312	7	36	218**	4	25	307	1	10
10	509**	24	56	448*	8	87	532**	4	78	389	1	5

* Indicates those depths where the above misfit is higher than 10%

** Indicates those inversion derived depths, which shows a deviation higher than 20% compared to depths estimated by 2.5D CGWI inversion

2.5D CGWI is the result of the 3D approximate CGWI, which is a 2D CGI joint inversion procedure using the data sets measured in both dip and strike directions and Steiner weights.

It is shown that the standard deviation of depths increases for 2D CGI (dip) inversion compared to 2.5D CGWI, as the former has more values that are outlying. The standard deviation is even higher for 2D CGI (strike) inversion, and it is the greatest for 1D single inversion. It is also demonstrated that the value of Y^* is normally higher than that of Y_n^*, which is due to the slight increase in overall depth estimation caused by large errors in thin layers. Similar functions describe the relation between the depths estimated by 2.5D CGWI and other inversion methods. The highest standard deviation and lowest correlation coefficient are shown by the result of 1D single inversion. The strongest correlation is between the results of 2.5D CGWI and 2D CGI (dip) inversion, which means that profile Profile-I basically shows a dip structure combined with strike features. VES data sets inverted by the 2D CGI method were collected along the dip direction. The 45-degree straight lines are promising for the reliability of inversion, but the outliers refer to a complicated structure resulting in significant uncertainty of the results of 2D CGI and especially 1D inversion.

The depth coordinates for the VES stations estimated by inversion are plotted in Fig. 7. The results of different inversion methods can be compared by using spline interpolation on the depth data.

Even if the use of splines creates a significant simplification for the Fourier expansion, we can draw three important conclusions:

1. The sections show significant depth variations around VES stations 5, 6 and 10.
2. Around the major structural changes, the depth values estimated by inversion show high scattering.
3. Despite the large differences between stations 5, 6 and 10, they all show major structural variability. These depth variations can be interpreted as fracture zones in hydroquarzitic tuff, above which a clayey decomposed tuff layer more than 100 m thick is situated. These structural zones may represent the places of thermal water

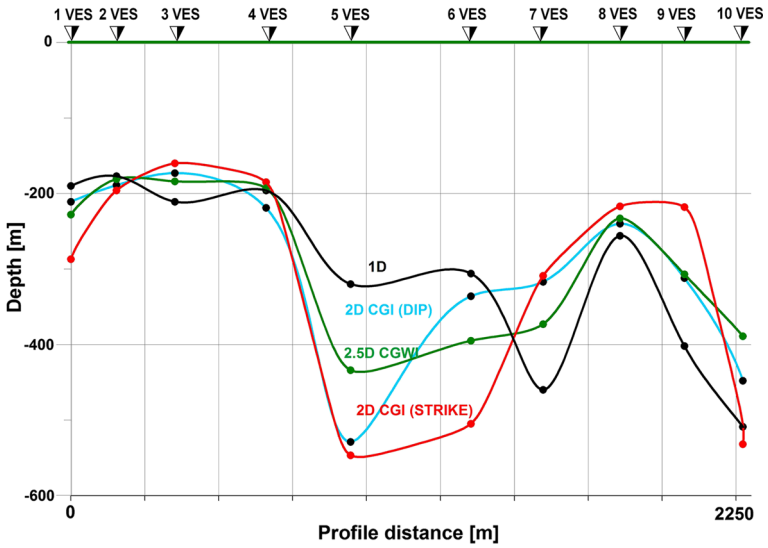

Fig. 7 Depth values in different VES stations along Profile-I

upwelling from which water could be exploited. North from the area presented in this study, there are several wells drilled into the same structural zones that produce water from a depth between 50 and 200 m.

3.2.3 Interpretation of Other Profiles (Profiles-0, II and III)

Figure 8 shows the apparent resistivity pseudosection made from the data of VES stations situated along Profile-0, which can be used to relate to the inversion results.

The result of the 2.5D CGWI of Profile-0 is shown in Fig. 9, which shows that the depth of the basement gradually decreases from 200 to 100 m between VES stations 1 and 20 northwards (from southwest to northeast direction) by traversing three or four faults. At VES station 20, the boundary of the basement changes quite smoothly, which hardly explains the drilling of an earlier (dry) 600-m prospecting well around this station.

The apparent resistivity pseudosection along Profile-II is presented in Fig. 10.

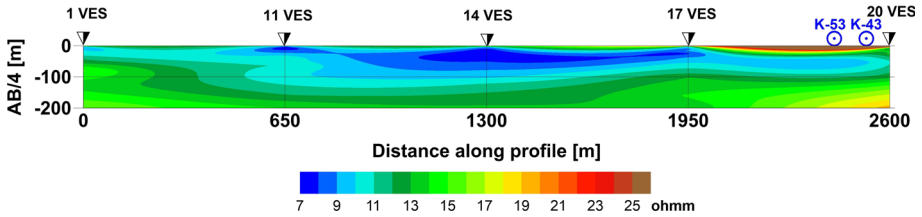

Fig. 8 Apparent resistivity pseudosection along Profile-0

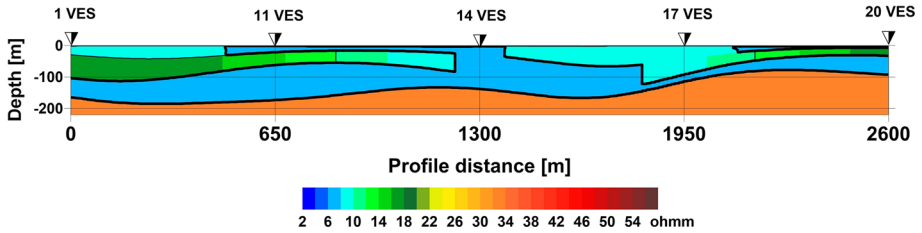

Fig. 9 Resistivity section estimated by 2.5D CGWI method along Profile-0

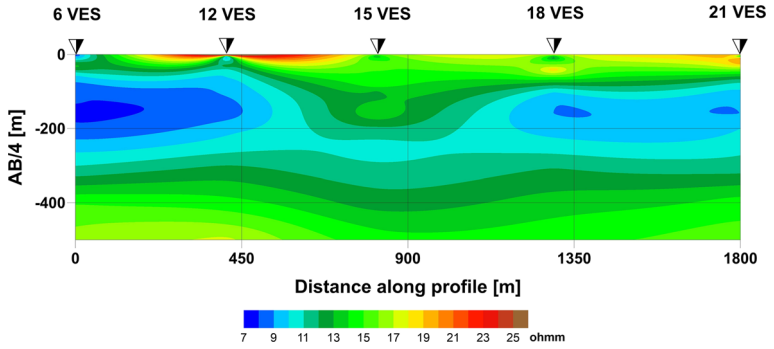

Fig. 10 Apparent resistivity pseudosection along Profile-II

The 2.5D CGWI results of Profile-II are plotted in Fig. 11, which shows a significant change in the geological structure around VES station 15. Five VES stations along Profile-II and III allow for the use of small number of expansion coefficients in the inversion procedure. It may partly cause a relatively low resolution, and at the same time, the 400- to 450-m station distance is also too long to achieve better resolution.

The apparent resistivity pseudosection and the result of 2.5D CGWI along Profile-III are presented in Figs. 12 and 13. The section refers to mainly a change in strike direction in the vicinity of VES stations 16, 19 and 22. In addition to Profiles-0, I, II, III, two VESs were also carried out in the vicinity of station 18. Since they could not be interpreted in any joint inversion procedures, the processing of these measurements was made by single inversion methods (VES stations 2/6 and 2/7). The results of single inversion were less accurate than those of the 2.5D CGWI method. These measurements were useful for drawing apparent resistivity maps for the regional interpretation. Because of the interpretation of sparse measurements, the northern parts of the isoline maps represented in Figs. 14, 15 and 16 show relatively low resolution, but their southern parts imply the existence of structures that could be of interest in planning where to drill a thermal water prospecting well. In this area, there are vertical structures (i.e., rifts and fractures) of measurable sizes (200–250 m).

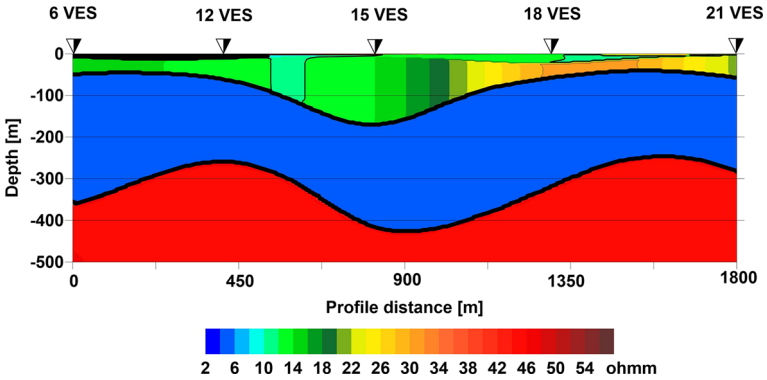

Fig. 11 Resistivity section estimated by 2.5D CGWI method along Profile-II

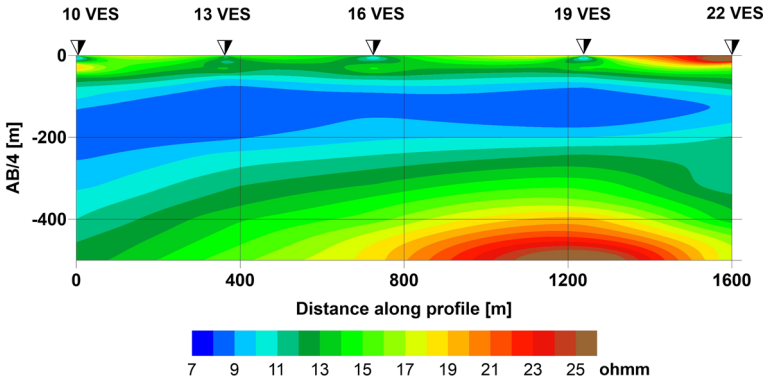

Fig. 12 Apparent resistivity pseudosection along Profile-III

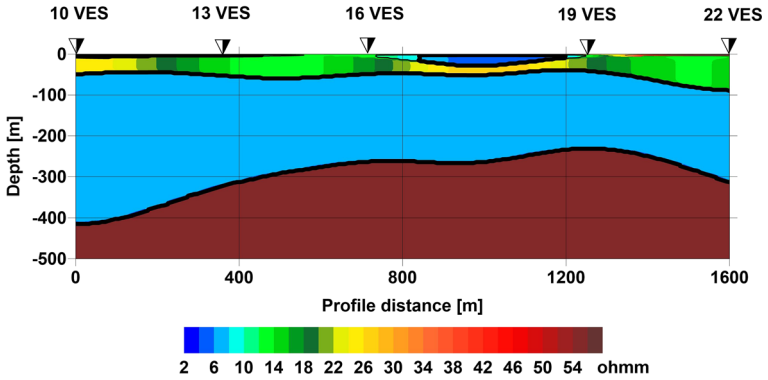

Fig. 13 Resistivity section estimated by 2.5D CGWI method along Profile-III

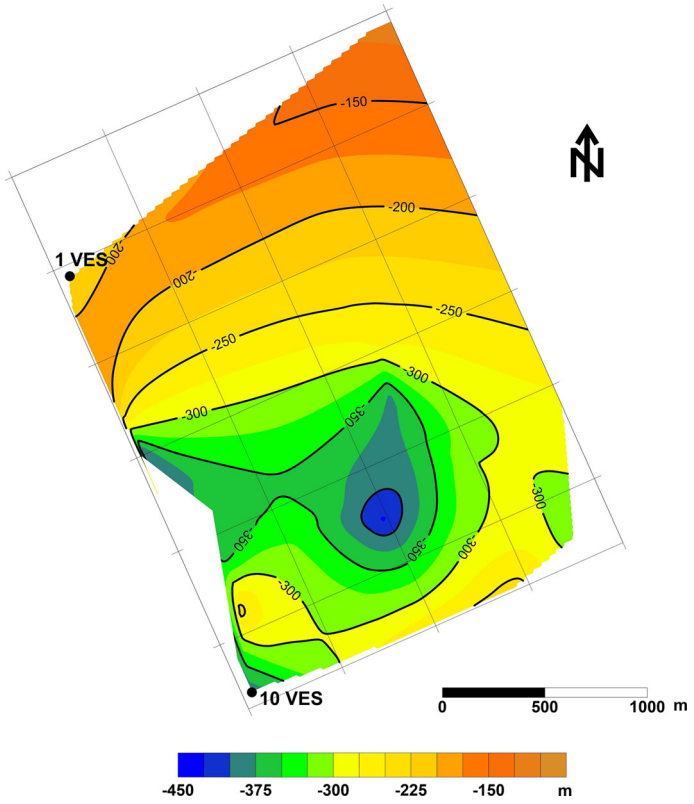

Fig. 14 Iso-depth map of volcanic aquifer estimated by 2.5D CGWI method

The cone-shaped structure with maximum depth of 200 m, shown in Fig. 16, is especially interesting. It looks like a volcanic vent filled out with younger sediments.

As a result of the geophysical survey and interpretation, the structural zones between VES stations 5–6 or VES stations 9–10 of Profile-I seem to be the most promising ones

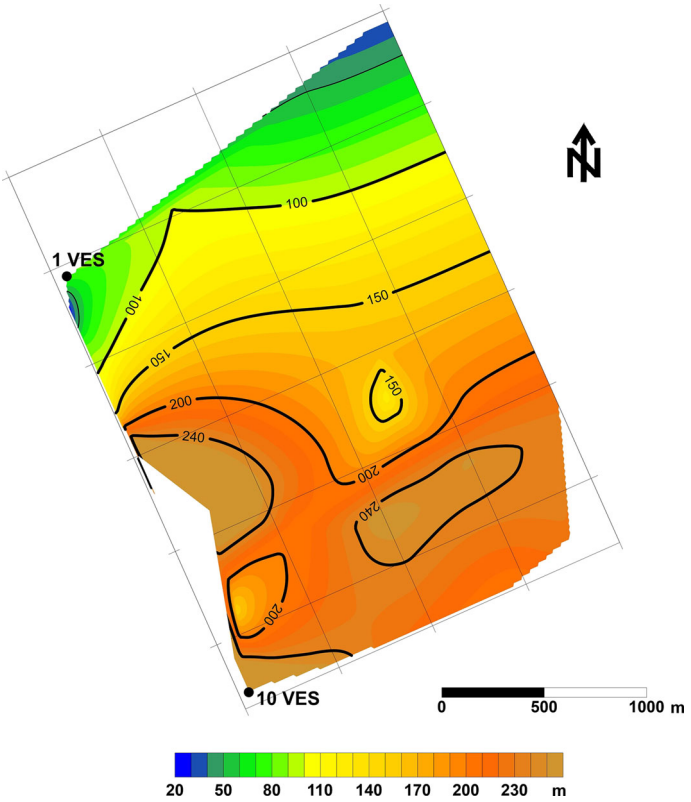

Fig. 15 Iso-thickness map of weathered ash rock estimated by 2.5D CGWI method

from the point of view of well location. Both of them have transversal east–west extensions. The area situated above the vent structure (at depth 400–450 m) may or may not be ideal for a prospecting well, although it was probably formed at the junction of transversal structures—favorable for an intensive magmatic up-flow.

4 Conclusions

Geoelectric methods can be widely used in geologic, hydrogeologic and environmental exploration. In this paper, the advantage of their practical use was highlighted. As a result of our series expansion-based geoelectric inversion method development work, after 1.5D, 2D CGI and 2D CGI methods, a new inversion method was developed, which allowed for the quality-checked determination of complicated (showing mixed features of 1D, 2D and 3D models) geological structures. This possibility has been proven by using synthetic modeling and field examples. According to the opinion of the authors, the single (1D) inversion method without using any quality information of the estimated model parameters can be applied only with great uncertainty. They insist upon also proving that the representation of measurement data in log–log scale and/or in the form of pseudosection may greatly help the interpretation process. In the case of areal measurements, both station offsets and profile distances must be harmonized with the depth of penetration to achieve

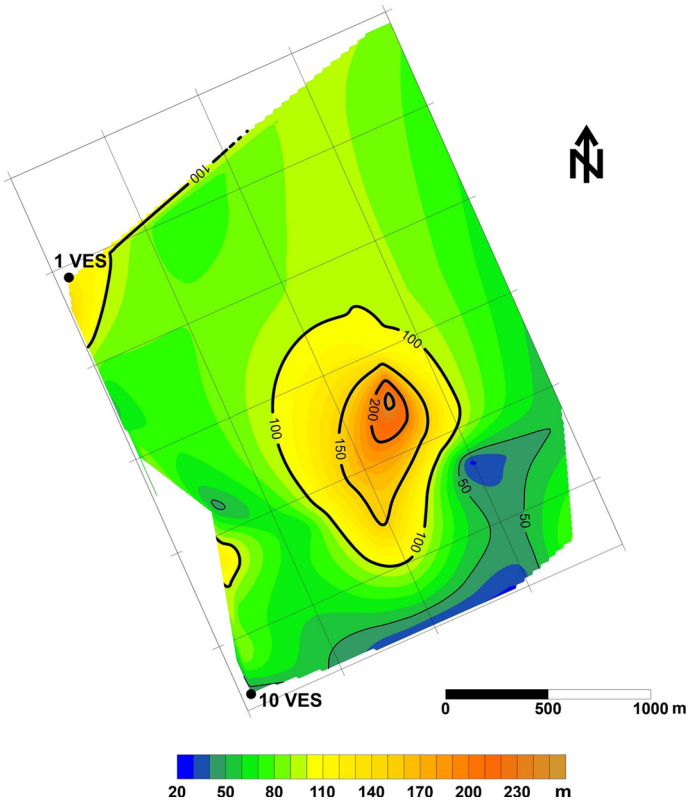

Fig. 16 Iso-thickness map of sediments overlying the weathered ash rock, estimated by 2.5D CGWI method

an optimal resolution. The developed geoelectric (i.e., 1D, 2D CGI and 2.5D CGWI) inversion methods allowed for the regional interpretation of VES data acquired in Szerencs and then the determination of the possible locations of thermal water prospecting wells.

Acknowledgements The research was supported by the GINOP-2.3.2-15-2016-00010 "Development of enhanced engineering methods with the aim at utilization of subterranean energy resources" project in the framework of the Széchenyi 2020 Plan, funded by the European Union, co-financed by the European Structural and Investment Funds. The research was partly supported by the Hungarian Research Fund OTKA (Project No. K109441). As participant researcher of the OTKA project, the first author is grateful for the support.

Appendix

For further interpretation of the depth analysis discussed in Sect. 3.2.2, Figs. 17 and 18 show more information. Figure 17 represents the relations between the depth estimation errors, while Fig. 18 shows the relations between the errors of depth parameter estimation. Both figures show that despite the high deviation between the depths and errors estimated by single 1D, 2D CGI (dip), 2D CGI (strike) and 2.5D CGWI procedures, there is a strong

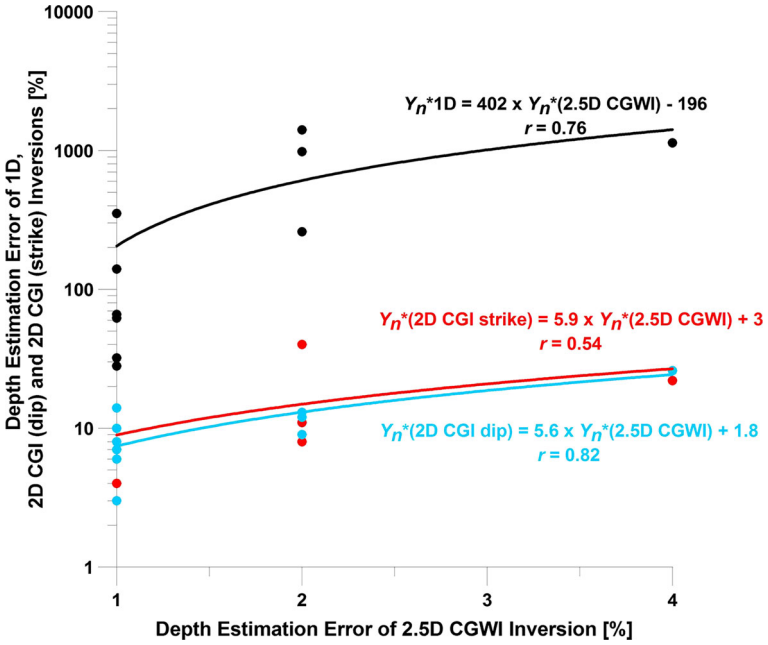

Fig. 17 Depth estimation errors obtained by 1D, 2D CGI (dip), 2D CGI (strike) inversion methods compared to that of 2.5D CGWI procedure

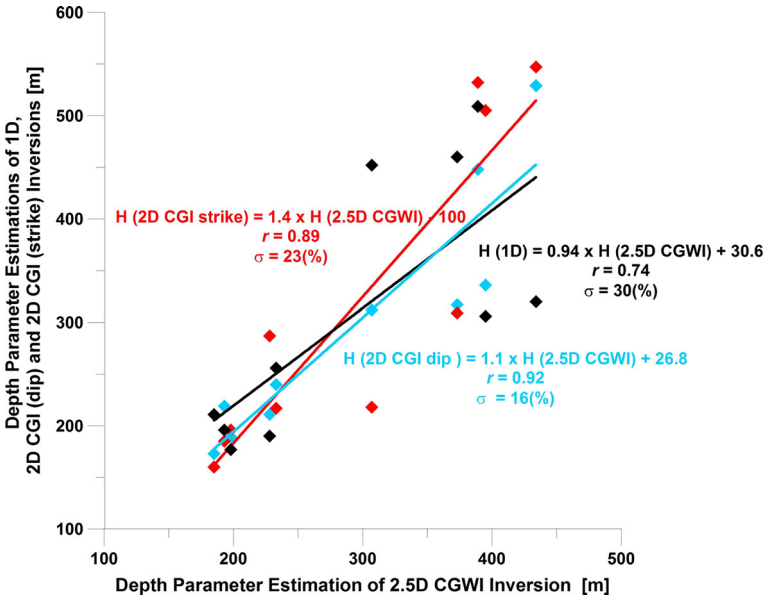

Fig. 18 Depth parameter errors obtained by 1D, 2D CGI (dip), 2D CGI (strike) inversion methods compared to that of 2.5D CGWI procedure

correlation between them, as shown by the high correlation coefficients (r). The deviation in regression coefficients in Fig. 18 is calculated by

$$\sigma^* = \frac{\sqrt{sq'd}}{\sqrt{\frac{\sum_{i=1}^{I} H_i^2}{n}}} \times 100\%, \tag{15}$$

where sq′d means the residual mean square of the layer thicknesses H ($H = h_1 + h_2 + h_3 + h_4$), i is the number of layers and n is the number of VES stations. (The above quantity is not the same as the estimation error of inversion-derived model parameters.) Not only relations between the depths but also those of the estimation errors are determined for the 2D dip and 2D CGI procedures using VES data measured along dip direction. There is an outstanding relation between the errors characterizing the quality of depth estimation of the inversion methods. The errors are listed in Table 3 (Sect. 3.2.2). A linear relation between the results of 2.5D CGWI and other inversion methods is observable here. For a better representation, the values were plotted on a logarithmic scale on the ordinate axis, which may bias the linear trend between the relevant variables. Values r ($r = 0.76$; 0.54; 0.82) refer to a function-like relationship (Fig. 17). We emphasize here the reliability of the estimation results of 2.5D CGWI, even when this approximation causes considerable bias.

References

Alpin LM, Berdichevskii MN, Vedsintsev GA, Zagarmistr AM (1966) Dipole methods for measuring earth conductivity. (Selected and translated from the Russian by Keller G.V.), Consultant Bureau, New York

Auken E, Christiansen AV (2004) Layered and laterally constrained 2D inversion of resistivity data. Geophysics 69:752–761

Auken E, Chrisiansen AV, Jacobsen BH, Foged N, Sorensen KI (2005) Piecewise 1D laterally constrained inversion of resistivity data. Geophys Prospect 53:497–506

Barker RD (1992) A simple algorithm for electrical imaging of the surface. First Break 10:53–62

Beard LP, Morgan FD (1991) Assessment of 2D resistivity structures using 1D inversion. Geophysics 56:874–883

Blaschek R, Hördt A, Kemna A (2008) A new sensitivity-controlled focusing regularization scheme for the inversion of induced polarization data based on the minimum gradient support. Geophysics 73:45–54

Bortoloza CA, Porsani ER, Almeida ER, Santos FAM (2011) 1D joint inversion of DC and TEM data for hydrogeological applications. In: Near surface 17th EAGE European meeting of environmental and engineering geophysics

Buvat S, Schamper C, Tabbagh A (2013) Approximate Threedimensional resistivity modelling using Fourier analysis of layer resistivity in shallow soil studies. Geophys J Int 194:158–169

Coggon JA (1971) Electromagnetic and electrical modeling by the finite-element method. Geophysics 36:132–155

Dey A, Morrison HF (1979a) Resistivity modelling for arbitrarily shaped two dimensional structures. Geophys Prospect 27:106–136

Dey A, Morrison HF (1979b) Resistivity modelling for arbitrarily shaped three dimensional structures. Geophysics 44:753–780

Dobróka M, Szabó PN (2005) Combined global/linear inversion of well-logging data in layer-wise homogeneous and inhomogeneous media. Acta Geod et Geophys Hung 40(2):203–214

Dobróka M, Völgyesi L (2008) Inversion reconstruction of gravity potential based on gravity gradients. Math Geosci 40(3):299–311

Dobróka M, Gyulai Á, Ormos T, Csókás J, Dresen L (1991) Joint inversion of seismic and geoelectric data recorded in an underground coal mine. Geophys Prospect 39:643–655

Dobróka M, Szabó PN, Cardarelli E, Vass P (2009) 2D inversion of borehole logging data for simultaneous determination of rock interfaces and petrophysical parameters. Acta Geod et Geophys Hung 44(4):459–479

Dobróka M, Szabó NP, Tóth J, Vass P (2016) Interval inversion approach for an improved interpretation of well logs. Geophysics 81(2):D163–D175
Doetsch J, Linde N, Coscia S, Greenhalgh SA, Green AG (2010) Zonation for 3D aquifer characterisation based on joint inversion of multimethod crosshole geophysical data. Geophysics 75(6):53–64
Drahos D (2008) Determining the objective function for geophysical joint inversion. Geophys Trans 45:105–121
Gallardo LA, Meju MA (2004) Joint two dimensional DC resistivity and seismic travel-time inversion with cross-gradients constraints. J Geophys Res 109(B3):3311–3321
Gandomi JA, Binley A (2013) A Bayesian Transdimensional approach for the fusion of multiple geophysical dataset. J Appl Geophys 96:38–54
Geotomo Software (2006) Res2DINV ver. 3.55 Malaysia. www.geoelectrical.com
Günter T, Rücker C, Spitzer K (2006) Three-dimensional modelling and inversion of dc resistivity data incorporating topography-II. Inversion. Geophys J Int 166(2):506–517. doi:10.1111/j.1365-246X.2006.03011.x
Gyulai Á, Ormos T (1996) Simultaneous inversion of geoelectric data for dipping beds based an analytical forward modelling (in hungarian). Magy Geofiz 37:17–26
Gyulai Á, Ormos T (1999) A new procedure for the interpretation of VES data: 1.5 D simultaneous inversion method. J Appl Geophys 41:1–17
Gyulai Á, Szabó NP (2014) Geoenvironmental investigation by series expansion based geoelectric inversion methodology. Front in Geosci 2(1):11–17
Gyulai Á, Tolnai ÉE (2012) 2.5D geoelectric inversion method using series expansion. Acta Geod et Geophys Hung 47(2):210–222
Gyulai Á, Ormos T, Dobróka M (2010) A quick 2D geoelectric inversion method using series expansion. J Appl Geophys 72(4):232–241
Gyulai Á, Turai E, Baracza MK (2012) The analysis of CGWI inversion results involving a field case (in Hungarian). Magy Geofiz 53(4):264–274
Gyulai Á, Baracza MK, Tolnai ÉE (2013) The application of joint inversion in geophysical exploration. Int J Geosci 4:283–289
Gyulai Á, Baracza MK, Szabó NP (2014) On the application of combined geoelectric weighted inversion in environmental exploration. Environ Earth Sci 71:383–392
Haber E, Oldenburg DW (1997) Joint inversion: a structural approach. Inverse Probl 13(1):63–77
Hering A, Misiek R, Gyulai Á, Ormos T, Dobróka M, Dresen L (1995) A joint inversion algorithm to process geoelectric and surface wave seismic data. Part I. Basic ideas. Geophys Prospect 43:135–156
Jegen M, Hobbs RW, Tartis P, Chave A (2009) Joint inversion of marine magnetotelluric and gravity data incorporating seismic constraints. Preliminary results of sub basalt imaging of the Farve Shelf. Earth Planet Sci Lett 282(1–4):47–95
Kis M, Gyulai Á, Ormos T, Dobróka M, Dresen L (1998) A new approach for the investigation of 2D structures-method development and case-history. In: 60th EAGE conference and technical exhibition, 8–12 June 1998
Kiss G (2007) The Zemplén-mountain protected area, the mountain's name, boundaries and landscapes (in hungarian). Bükk Publisher, Eger, pp 9–12
Koefoed O, Mallick K (1979) Geosounding principles 1, resistivity sounding measurements. Elsevier, Amsterdam
Kumar R, Das UC (1978) Transformation of Schlumberger apparent resistivity to dipole apparent resistivity over layered earth by the application of digital linear filters. Geophys Prospect 26:352–358
Lee T (1975) An integral equation and its solution for some two- and three-dimensional problems in resistivity and induced polarisation. Geophysics 42:81–95
Li Y, Oldenburg DW (1994) Inversion of 3D DC resistivity data using an approximate inverse mapping. Geophys J Int 116:527–537
Loke MH, Barker RD (1996) Rapid least-squares inversion of apparent resistivity pseudosections by a quasi-Newton method. Geophys Prospect 44:131–152
Meheni Y, Guerin R, Benderitter Y, Tabbagh A (1996) Surface DC resistivity mapping: approximate 1D interpretation. J Appl Geophys 34:255–270
Menke W (1984) Geophysical data analysis—discrete inverse theory. Academic Press, London
Misiek R, Liebig A, Gyulai Á, Ormos T, Dobróka M, Dresen L (1997) A joint inversion algorithm to process geoelectric and surface wave seismic data. Part II. Application. Geophys Prospect 45:65–85
Mufti IR (1976) Finite difference resistivity modelling for arbitrarily shaped two-dimensional structures. Geophysics 46:1148–1163
Olainka AI, Weller A (1997) The inversion of geoelectrical data for hydrogeological application in crystalline basement areas of Nigeria. J Appl Geophys 37:103–115

Sasaki Y (1994) 3D resistivity inversion using the finite-element method. Geophysics 57:1270–1281
Spitzer K (1995) A 3D finite difference algorithm for DC resistivity modelling using conjugate gradient methods. Geophys J Int 123:902–914
Steiner F (1988) Most frequent value procedures. (short monograph). Geophys Trans 34:139–260
Steiner F (1991) The most frequent value. Introduction to a modern conception of statistics. Academic Press, Budapest. ISBN 9630556871
Steiner F (1997) Optimum methods in statistics (English). Akadémiai Kiadó, Budapest. ISBN 963057439X
Szabó NP (2004) Global inversion of well log data. Geophysical Transactions, vol 44, no 3–4, pp 313–329, HU ISSN 0016-7177
Szabó NP (2015) Hydraulic conductivity explored by factor analysis of borehole geophysical data. Hydrogeol J (online first article). doi:10.1007/s10040-015-1235-4
Szabó NP, Balogh GP (2016) Most frequent value based factor analysis of engineering geophysical sounding logs. In: 78th EAGE conference and exhibition 30 May–2 June 2016, paper: Tu SBT412
Székely F, Szűcs P, Zákányi B, Cserny T, Fejes Z (2015) Comparative analysis of pumping tests conducted in layered rhyolitic volcanic formations. J Hydrol 520:180–185
Szűcs P, Fejes Z, Szlabóczky P (2013) Hydrogeophysical research in the southern part of the Tokaj mountains (in Hungarian). Technical sciences of the north-east region in Hungary Debrecen, technical professional committee of academic committee of Debrecen, electronic technical papers XII, pp 66–73
Tripp AC, Holmann GW, Swift CM (1984) Two-dimensional resistivity inversion. Geophysics 49:1708–1717
Vozoff K, Jupp DLB (1975) Joint inversion of geophysical data. Geophys J R Astron Soc 42:977–991